applied sciences

MDPI

Article

A GA and SVM Classification Model for Pine Wilt Disease Detection Using UAV-Based Hyperspectral Imagery

Sulan Zhang [1,2,3,4,*], Hong Huang [2,*], Yunbiao Huang [1], Dongdong Cheng [3] and Jinlong Huang [3]

1 The Technical Center of Chongqing Chuanyi Automation Co., Ltd., Chongqing 401121, China; hybmail@163.com
2 Key Laboratory of Optoelectronic Technology and Systems of the Education Ministry of China, Chongqing University, Chongqing 400044, China
3 College of Big Data and Intelligent Engineering, Yangtze Normal University, Chongqing 408100, China; cdd@cqu.edu.cn (D.C.); hjl@yznu.edu.cn (J.H.)
4 Hyperspectral Remote Sensing Monitoring Center for Ecological Environment of the Three Gorges Reservoir Area, Yangtze Normal University, Chongqing 408100, China
* Correspondence: slzhang@cqu.edu.cn (S.Z.); hhuang.cqu@gmail.com (H.H.)

Abstract: Pine wilt disease (PWD), caused by the pine wood nematode (*Bursaphelenchus xylophilus*), is a global destructive threat to forests and has led to serious economic losses all over the world. Therefore, it is necessary to establish a feasible and effective method to accurately monitor and estimate PWD infection. In this study, we used hyperspectral imagery (HI) collected by an unmanned airship with a hyperspectral imaging spectrometer to detect PWD in healthy, early, middle and serious infection stages. To avoid massive calculations on the full spectral dimensions of the HI, 16 spectral features were extracted from the HI, and a genetic algorithm (GA) was implemented to identify the optimal ones with the least fitness. Simultaneously, a support vector machine (SVM) classifier was established to predict the PWD infection stage for an individual pine tree. The following results were obtained: (1) the spectral characteristics for pine trees in different PWD infection stages were distinctive in the green region (510–580 nm), red edge (680–760 nm) and near-infrared (780–1000 nm) spectra; (2) the six optimal spectral features (D_{green}, SD_{green}, D_{red}, D_{RE}, D_{NIR}, SD_{NIR}) selected with the GA effectively distinguished the PWD infection stages of pine trees with a lower calculation cost; (3) compared with the traditional classifiers, such as k-nearest neighbor (KNN), random forest (RF) and single SVM, the proposed GA and SVM classifier achieved the highest overall accuracy (95.24%) and Kappa coefficient (0.9234). The approach could also be employed for monitoring and detecting other forest pests.

Keywords: pine wilt disease; hyperspectral imagery; GA; SVM; classification

Citation: Zhang, S.; Huang, H.; Huang, Y.; Cheng, D.; Huang, J. A GA and SVM Classification Model for Pine Wilt Disease Detection Using UAV-Based Hyperspectral Imagery. *Appl. Sci.* **2022**, *12*, 6676. https://doi.org/10.3390/app12136676

Academic Editor: Seong-Ik Han

Received: 20 May 2022
Accepted: 28 June 2022
Published: 1 July 2022

1. Introduction

Pine trees are important sources of forest products and play other important roles in environmental protection such as preventing wind and sand breaks and landslides, especially in East Asian countries [1]. Parts of the trees are regularly being used as dietary supplements because of their several health and medicinal benefits [2,3]. However, pine trees are facing a serious and destructive disease, pine wilt disease (PWD), which is caused by the pine wood nematode (PWN, *Bursaphelenchus xylophilus*) and is spread through the insect vector pine sawyer beetle (*Monochamus* spp.) [4]. PWD first appeared in North America but is now widely found around the world [5–7]. As most pine trees infected by PWD die within three months, PWD has caused significant economic losses and adverse environmental impacts in China since its first appearance in 1982 in Nanjing [8].

To effectively refrain PWD spread, current control methods usually identify the PWD-infected pine trees through field survey and use fumigation, burning and tree-felling operations when the onset outbreak occurs [9,10]. However, pine trees usually grow

in large mountain areas and communities, which make standard ground identification and sampling methods time- and labor-consuming and sometimes even impractical. To overcome those difficulties, hyperspectral remote sensing (HRS) technology, which can obtain continuous spectral information of objects, has been explored to examine the impact of PWD on the physiological and biochemical changes after infection [11]. According to the data acquisition scale, research on the remote sensing monitoring of PWD is mainly divided into three classes, including ground remote sensing, high-altitude remote sensing and low-altitude remote sensing [12].

Ground remote sensing reveals that the presence of PWD significantly correlates with hyperspectral features. Zhang et al. [13] showed that the spectral reflectance of Pinus Massoniana in different stages of PWD appeared to be greatly different. Kim et al. [14] constructed a green-red spectral area index (GRSAI) and found that it detected PWD infection faster than other indices. However, those studies used a field portable spectrometer to collect spectral data and neglected spatial information and therefore could not be applied in a large-scale area [15]. High-altitude remote sensing usually uses satellite imagery from Landsat, Spot, WorldView and BJ-2 to detect PWD [16]. Zhang et al. [17] proposed a spatiotemporal change detection method to reduce false detections in tree-scale PWD monitoring in a complex landscape. Li et al. [18] retrieved PWD-infected areas from medium-resolution satellite images based on the simulations of an extended stochastic radiative transfer model. However, due to the limitations of low spatial–temporal resolutions and weather complications, high-altitude remote sensing methods usually achieve low PWD detection accuracy [19].

Compared with ground remote sensing and high-altitude remote sensing, low-altitude remote sensing with unmanned aerial vehicles (UAVs) is flexible and efficient and has the advantage of yielding low-cost, high-spatial-resolution, and high PWD detection accuracy [20,21]. The HI generated by a UAV hyperspectral imaging spectrometer has great potential in detecting PWD with its abundant spatial and spectral information [22–24]. Huang et al. [25] used a fixed-wing UAV equipped with a multispectral digital camera to collect the normalized differential vegetation index (NDVI) of pine trees and recognized the dead pine trees caused by PWD with 80% accuracy. Li et al. [26] successfully recognized PWD-infected pine trees with 90.4% accuracy using the color characteristics of UAV remote-sensing images. Abdel-Rahman et al. [27] explored SVM and RF classifiers to distinguish pine trees in healthy, Sirex noctilio grey-attacked and lightning-damaged stages with airborne hyperspectral data. However, the above works have not explored the advantages of hyperspectral data in identifying PWD infection stages.

Although many machine learning algorithms have been explored to detect PWD in its early stages with UAV remote sensing, they usually focus on the RGB image or a few spectral bands from a multispectral image [9,12] and fail to simultaneously extract and fully utilize the spatial and spectral information in HI. Meanwhile, there are a few studies that provide good spectral features to identify pine trees in the healthy, early, middle and serious PWD infection stages. Iordache et al. [28] found that random forest with airborne hyperspectral data performed well in identifying the infected, suspicious and healthy trees. Therefore, this study intends to explore the GA and SVM machine learning algorithms with UAV hyperspectral imagery to predict the PWD infection stages for pine trees with high accuracy.

The remainder of this paper is organized as follows. Section 2 briefly describes the materials' preparation. The details of the GA and SVM classification model are introduced in Section 3. Section 4 presents the experiment results, which demonstrate the effectiveness of the proposed method. Finally, Sections 5 and 6 are the discussion and conclusion parts.

2. Materials

2.1. Study Area

The study site is located in the north of Fuling district, Chongqing City of southwest China (106°56′–107°43′ E, 29°21′–30°01′ N; Figure 1), which has a mid-subtropical humid

monsoon climate. The altitude and the mean annual air temperature of the study site are 300–1977 m and 16–22 °C, respectively, which is suitable for pine tree growth. In our study, the tree farm is mainly composed of Pinus massoniana trees.

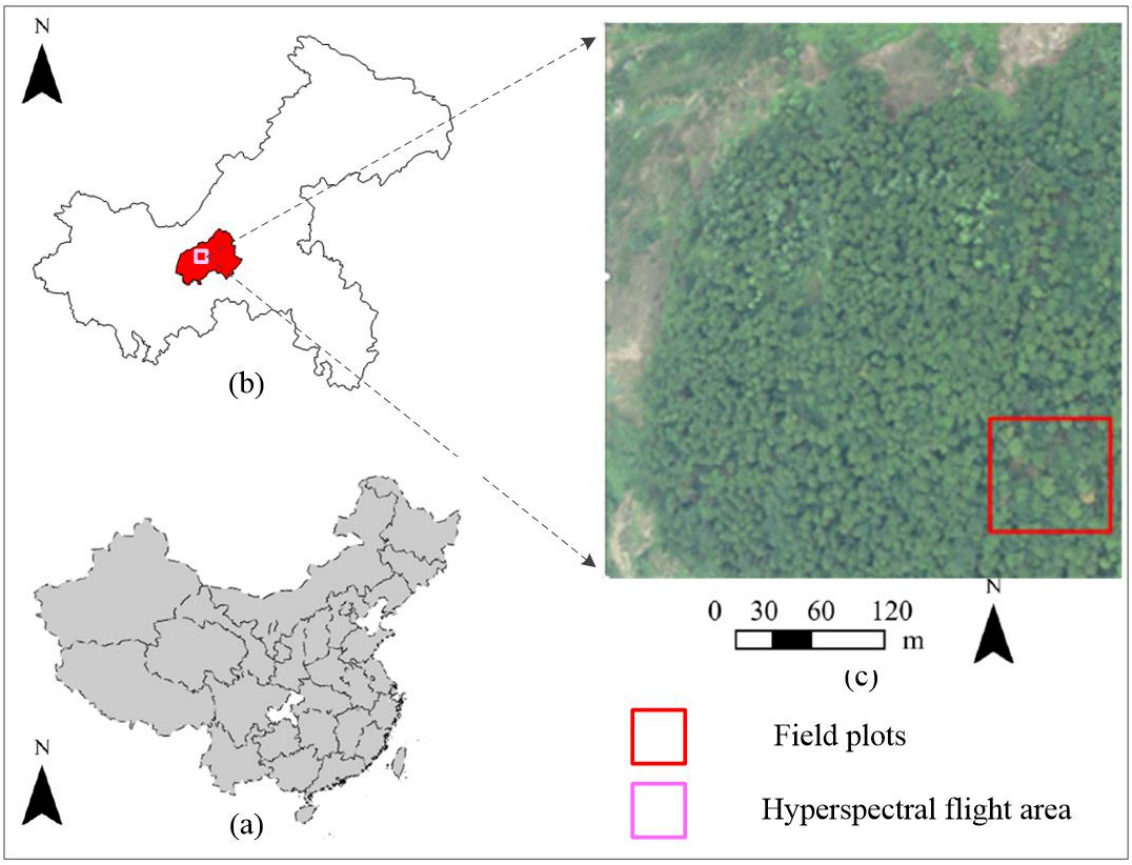

Figure 1. The study site location. (**a**) The map of China with Chongqing City in white color; (**b**) The map of Chongqing city with Fuling district in red color; (**c**) The UAV image of the study area. The purple rectangle in (**b**) and red rectangle in (**c**) represent the field plot's location and the hyperspectral flight area, respectively.

2.2. UAV-Based HI

At present, the HI is usually acquired by a low-altitude remote-sensing platform UAV, such as an unmanned fixed-wing aircraft, unmanned helicopter or unmanned airship equipped with a hyperspectral imaging spectrometer. Compared with the unmanned fixed-wing aircraft and the unmanned helicopter, the unmanned airship has the outstanding advantages of a long continuous flight time and high suspension and load abilities [21]. In our study, the HI (Figure 2) was collected by the UAV hyperspectral remote sensing system consisting of an unmanned airship, an automatic rudder system, a task device and a ground control system. The automatic rudder system consisted of a global positioning system (GPS), a computer and a gyroscope, while the task device consisted of a triaxial platform and a near-infrared hyperspectral imaging spectrometer, Hyperspec^{TM} VNIR (Headwall, MA, USA) with a 400–1000 spectral range, 325 bands and the EMCCD detector generating a 1004 × 1002 spatial image with 8 μm pixel size. The hyperspectral remote-sensing system communicated with the ground control system wirelessly.

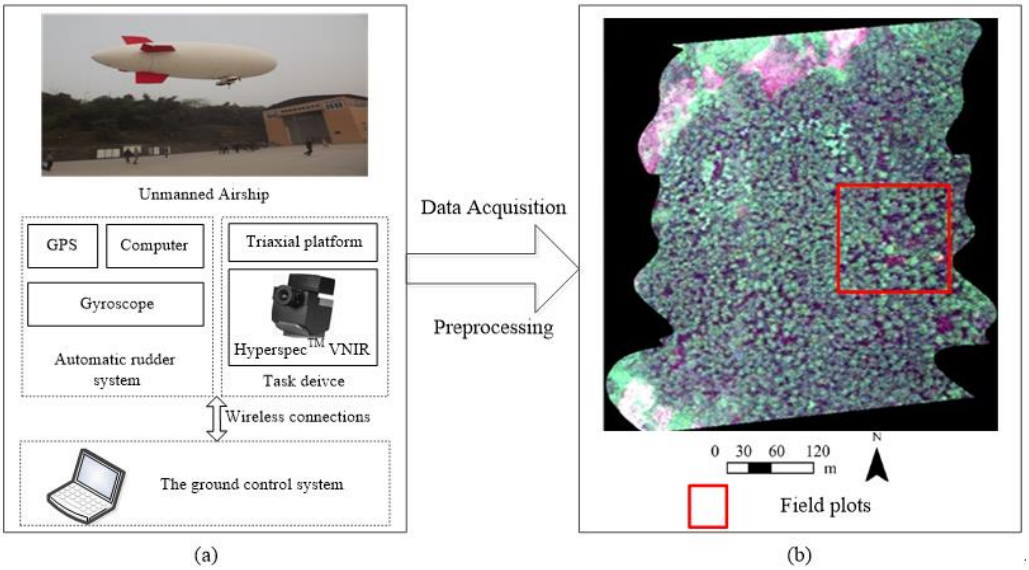

Figure 2. The HI acquisition: (**a**) UAV hyperspectral remote sensing system; (**b**) The HI acquired with UAV hyperspectral remote sensing system and preprocessing.

The survey shows that PWD usually spreads fast during May to December, and the physiological characteristics of infected pine trees change obviously [29]. Therefore, the HI data were collected for 30 min (4:30–5:00 PM) on 14 September 2020. The flight altitude was 112 km, and the ground resolution was 0.1 m. A total of 325 spectral channels from visible to near-infrared regions (400–100 nm) were included in the HI. In the preprocessing, radiometric correction was conducted using a diffuse reflection board and a Compact Hyperspectral Data Processing Unit (CHDPU) of Hyperspec^{TM} VNIR (Headwall, Bolton, MA, USA). Orthophotos, atmospheric and reflectance correction were also performed in the CHDPU.

2.3. Tree Crown Segmentation from HI

We segmented the pine tree crowns from the HI with a watershed algorithm [30] covering the following steps. Firstly, an NDVI index calculation and morphological filtering were operated on the original UAV-based HI, and a significant regional image of the canopy was obtained. Secondly, a vertex and its range of the canopy were extracted from the salient regional images as markers, and the tags were added to the gradient image; then, a watershed algorithm based on marker control was used to divide the canopy. Thirdly, the shadow components and overlapping crowns were abandoned. Based on the watershed algorithm, the pine trees that were missed and delineated incorrectly were delineated manually. Finally, the hyperspectral data of an individual pine tree was calculated by averaging the reflectance of each tree crown.

2.4. Infection Stage Categorization of Pine Tree

As described in previous studies, the physiological characteristics of pine trees change gradually with PWD infection aggravation [31,32]. According to the needle color and the resin secretion of pine trees, we characterized PWD infection into four stages with samples collected from field surveys by four experts in PWD research: (1) a healthy stage with green needles and normal resin secretion; (2) an early stage with needles beginning to turn yellow and resin secretion decreasing; (3) a middle stage with needles turning yellow and resin secretion obviously decreasing; and (4) a serious stage with reddish brown needles and no resin secretion. The needle samples, collected from pine trees in the study area in different PWD infection stages, are shown in Figure 3.

Figure 3. Pine tree needles in different infection stages collected from field survey and labeled by experts: (**a**) healthy stage; (**b**) early stage; (**c**) middle stage; (**d**) serious stage.

3. Method

3.1. Spectral Feature Extraction

After the pine tree crowns segmentation of the HI from the research area, the spectral reflection for each pine tree was calculated with the average of the crown hyperspectral data. Then, a Savitzky–Golay filter with points ranging from 3 to 15 was chosen in order to smooth the pine tree's spectral reflection [33]. When the pine tree suffers from PWD, its chlorophyll, water content and the cell structure in the needles change dramatically, leading to changes in the spectral reflectance. In general, the spectral reflection curves for pine trees in different PWD infection stages (Figure 4) reach their local peaks in the green region (GR, 510–580 nm), red edge (RE, 680–760 nm) and the near-infrared (NIR, 780–1000 nm) and reach their local valleys in the red region (RR, 620–680 nm). Based on those PWD-sensitive regions, we extracted 16 spectral features shown in Table 1 from the pine tree spectral reflection data, where ρ and ρ′ are the spectral reflectance and its first-order derivative.

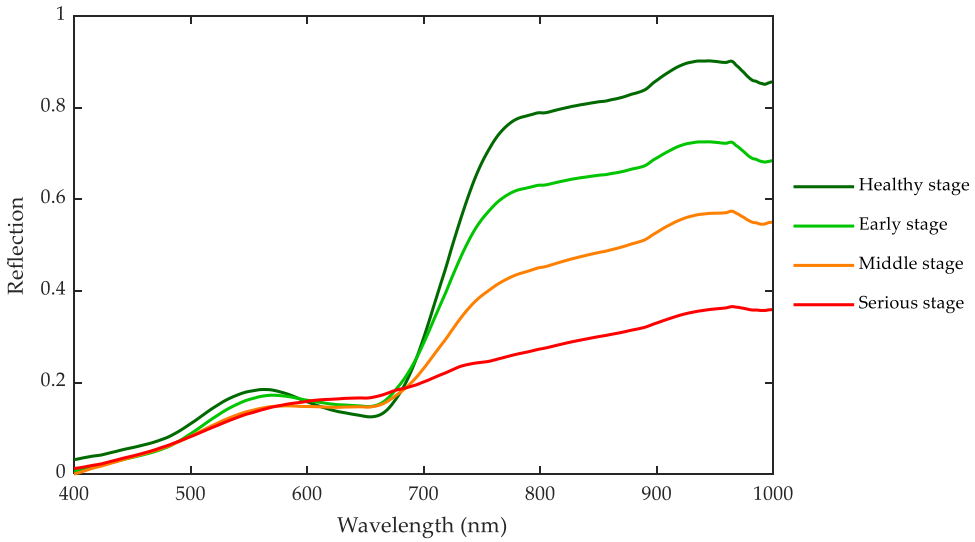

Figure 4. The spectral reflection curves of pine trees in different PWD infection stages, which were collected from HI with UAV hyperspectral remote-sensing system.

Table 1. 16 Spectral features defined on the spectral reflection data.

Variables	Description	Formula
R_{green}	Reflectance at green peak [34]	MAX ρ(510:580)
SR_{green}	Total reflectance in GR [35]	SUM ρ(510:580)
R_{red}	Reflectance at red valley [34]	MIN ρ(620:680)
SR_{red}	Total reflectance in RR [35]	SUM ρ(620:680)
R_{RE}	Reflectance at RR peak [35]	MAX ρ(680:760)
SR_{RE}	Total reflectance in RR [35]	SUM ρ(680:760)
R_{NIR}	Reflectance at NIR peak [35]	MAX ρ(780:1000)

Table 1. *Cont.*

Variables	Description	Formula
SR_{NIR}	Total reflectance in NIR [35]	SUM ρ(780:1000)
D_{green}	Max first-order derivative of the reflectance in GR [36]	MAX ρ′ (510:580)
SD_{green}	Total first-order derivative of the reflectance in GR [36]	SUM ρ′ (510:580)
D_{red}	Max first-order derivative of the reflectance in RR [36]	MAX ρ′ (620:680)
SD_{red}	Total first-order derivative of the reflectance in RR [36]	SUM ρ′ (620:680)
D_{RE}	Max first-order derivative of the reflectance in RE [37]	MAX ρ′ (680:760)
SD_{RE}	Total first-order derivative of the reflectance in RE [37]	SUM ρ′ (680:760)
D_{NIR}	Max first-order derivative of the reflectance in NIR [37]	MAX ρ′ (780:1000)
SD_{NIR}	Total first-order derivative of the reflectance in NIR [37]	SUM ρ′ (780:1000)

3.2. Coding Spectral Features in GA

According to the analysis in the above subsection, it is known that the PWD infection stages of the pine trees are related to the spectral features, but the 16 spectral features extracted do not always work well together in the detection of PWD infection in pine trees. Some spectral features may correlate with each other, leading to lower PWD infection detection accuracy and higher complexity. Therefore, GA, a general adaptive optimization methodology [38], is imported to adaptively search for the optimal spectral features for the PWD infection detection step. In GA, each spectral feature defined in Table 1 is coded as a type of gene in the chromosome shown in Equation (1):

$$\mathrm{Ch} = [R_{green}, SR_{green}, \ldots, D_{NIR}, SD_{NIR}] \quad (1)$$

All 16 extracted spectral features are coded using a binary system. When a spectral feature is selected by the chromosome, its gene value in the chromosome is set to 1 and 0 otherwise. At the beginning, chromosome *Ch* is randomly initialized to generate a set of candidate solutions for the population of the GA. Then, in each evolution step, successive populations are generated with the crossover operations under the fittest survival. Finally, the optimal spectral features are those which are set as 1 in the chromosome of the GA evolution results.

3.3. GA-SVM Classification Model

For the PWD infection stage detection of pine trees, we introduce SVM, originally proposed by Cortes and Vapnik [39], to build a classification model. SVM is a non-parametric machine learning method based on statistical learning theory and structural risk minimization. To adaptively obtain the optimal spectral features, we define a fitness function (Equation (2)) to assess the importance of a spectral feature in the GA evaluation step. Crossover and mutation functions are the main operations that randomly impact the fitness from step to step. The chromosome with the highest fitness will be selected into the recombination pool using the roulette wheel or the tournament selection methods:

$$\mathrm{Fitness}(\mathrm{Ch}) = \frac{\mathrm{Cov}(\mathrm{y}(\mathrm{Ch}), \hat{\mathrm{y}})}{\sqrt{\mathrm{Var}(\mathrm{y}(\mathrm{Ch}))}\sqrt{\mathrm{Var}(\hat{\mathrm{y}})}} \quad (2)$$

where y(Ch) is the predicted PWD infection stage from the SVM classification model for chromosome Ch in the GA, and $\hat{y}$ is the measured PWD infection stage in the data acquisition. Cov(y(Ch), $\hat{y}$) is the covariance between y(Ch) and $\hat{y}$, while Var(y(Ch)) and Var($\hat{y}$) are variances for y(Ch) and $\hat{y}$, respectively. Usually, the higher the fitness value, the better the spectral feature selection in the chromosome. With the fitness function, the optimal spectral features are determined and then used to train the SVM classification model for predicting the PWD infection stages of pine trees extracted from the HI.

3.4. Evaluation for the Classification Model

To inspect the accuracy of the classification model, we used a confusion matrix to calculate the accuracy metrics. A confusion matrix, also known as a contingency table or error matrix, is used to present the visualization effect of the classification algorithms' performance. Each column represents the predicted value, and each row presents the actual category. It consists of true positives (TP), true negatives (FN), false positives (FP) and false negatives (TN), which are defined in Table 2. Furthermore, the user accuracy (UA), producer accuracy (PA), overall accuracy (OA) and Kappa coefficient are all defined by the confusion matrix and specified in Table 2.

Table 2. Accuracy metrics for the classification model.

Name	Formula	Description
TP	True positive	True value is positive, and the number that the model considers is positive.
FN	False negative	True value is positive, and the number that the model considers is negative.
FP	False positive	True value is negative, and the number the model considers is positive.
TN	False negative	True value is negative, and the number that the model considers is negative.
User accuracy (UA)	TP/(TP + FP)	The proportion of the correctly predicted number to the total number of a class.
Producer accuracy (PA)	TP/(TP + FN)	The proportion of the correctly predicted number to the positive number of a class.
Overall accuracy (OA)	(TP + TN)/(TP + TN + FP + FN)	The proportion of total correctly predicted number to the total observed number.
Kappa coefficient (KAPPA)	(Po − Pe)/(1 − Pe), where Po = OA, Pe = ((TN + FN) × (TN + FP) + (FP + TP) × (FN + TP))/(TN + TP + FN + FP)^2	The kappa coefficient is used for consistency testing, and the calculation of the kappa coefficient is based on the confusion matrix.

4. Results

4.1. Experiment Environment and Dataset

The pine tree crown segmentation algorithm, the GA algorithm and the SVM classification model training and testing were conducted with the Matlab toolbox based on the SVM framework, libsvm. The experimental operation platform incorporated an Intel(R) Core i7 series CPU, RAM 16.0 GB. In the tree crown segmentation, we used a watershed algorithm to recognize the pine tree crowns from the HI and found that the segmentation accuracy was more than 80% compared with manual visual interpretation using ArcGIS software. Then, we manually delineated the trees that were missed or delineated incorrectly and calculated the spectrum of an individual pine tree by averaging the reflectance of each tree crown. Finally, 56 pine tree samples were extracted and labeled as healthy, early, middle or serious PWD infection stages with the aid of experts. The segmentation and labeling results are shown in Figure 5. In the classification process, the dataset was randomly split into two parts, 35 samples for model training and 21 samples for model testing.

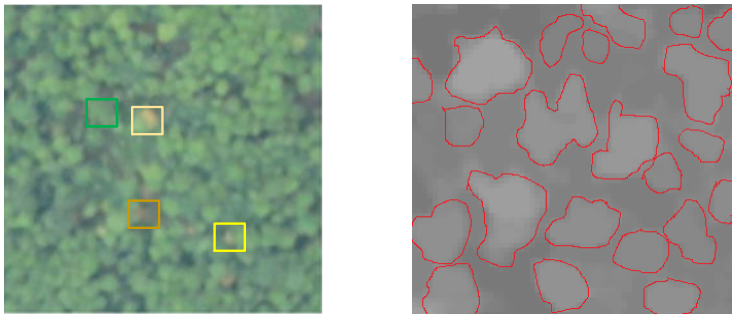

(a) (b)

Figure 5. The pine tree crown segmentation and labelling results: (**a**) pseudo color image of HI; (**b**) part segmentation result of HI shown in (**a**). The green, light yellow, yellow and brown circles represent the pine tree crowns in healthy, early, middle and serious PWD infection stages, respectively. The red circles represent the final segmentation of the pine trees.

4.2. Optimal Spectral Feature Selection

For selecting optimal spectral features, the parameters in the GA algorithm including the initial population size, the chromosome pairs' crossover probability, the mutation probability and the evolution times were initialized as 100, 0.6, 0.01 and 100, respectively, according to the empirical values from [38]. In the evolution, the chromosomes in the population did not change after 80 iterations, at which point the GA and SVM algorithm stopped, and the optimal spectral features were determined with Ch = [0000000011101011] and highest fitness. Then, six spectral features, including D_{green}, SD_{green}, D_{red}, D_{RE}, D_{NIR} and SD_{NIR}, were used for training the SVM classification model to predict the PWD infection stages of pine trees extracted from the HI.

The change trends of the six selected spectral features with the PWD infection stages for the dataset are illustrated in Figure 6. The D_{green} and D_{RE} decrease with the PWD infection stages, indicating that the reflectance of the pine trees in the healthy stage changes the most while the reflectance of the pine trees in the serious stage changes the least, which is consistent with the change trends of the spectral curves in Figure 4. The SD_{green}, D_{red}, D_{NIR} and SD_{NIR} for pine trees in the early PWD infection stages are higher and decrease with the PWD infection stages for other pine trees. These change trends indicate that the six optimal spectral features could extract the reflectance changes for the pine trees in different PWD infection stages well.

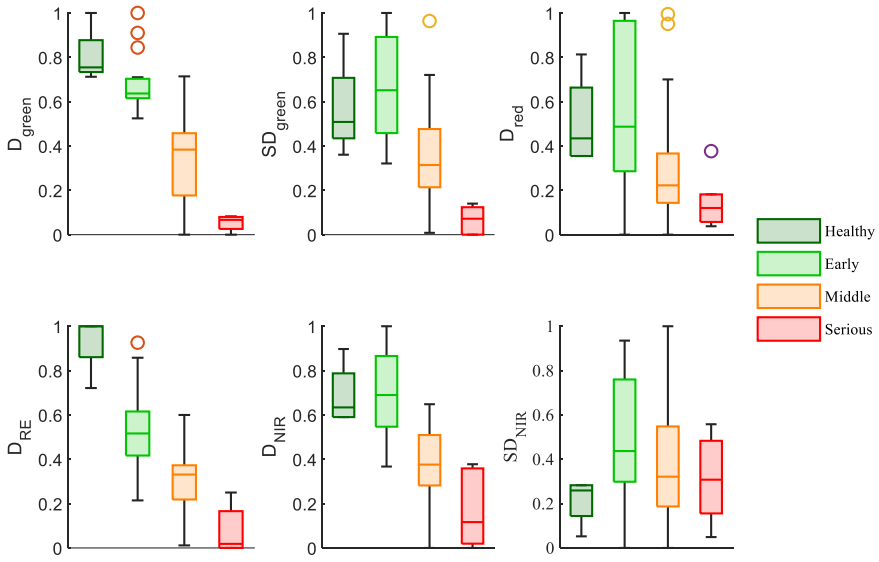

Figure 6. Comparison the six spectral features selected in GA at different PWD infection stage.

4.3. Classification Model Performance

To measure the proposed classification model performance, we introduced other machine learning algorithms, including KNN, RF and single SVM, which are frequently used for classification [4,9,40]. Then, we used the classification matrices including the PA, UA, OA and KAPPA coefficient defined in Table 2 to evaluate the performance. Usually, the higher the values of PA, UA, OA and KAPPA, the more precise the classification model is. The PWD infection stage detection results with hyperspectral data from KNN, RF, SVM and the proposed GA and SVM classification models are listed in Tables 3 and 4.

Table 3. The producer's accuracy (PA) and user's accuracy (UA) in different PWD infection stages using KNN, RF, SVM and GA and SVM model.

Model	Healthy Stage		Early Stage		Middle Stage		Serious Stage	
	PA(%)	UA(%)	PA(%)	UA(%)	PA(%)	UA(%)	PA(%)	UA(%)
KNN	0	NAN	100	62.5	91.67	84.62	0	NAN
RF	0	0	80	50	83.33	100	100	100
SVM	100	100	100	71.43	83.33	90.91	50	100
GA and SVM	100	100	100	100	91.67	100	100	66.67

Table 4. The overall accuracy (OA) and the Kappa coefficient for different classification models.

Model	OA(%)	KAPPA
KNN	76.19	0.5714
RF	76.19	0.6182
SVM	85.71	0.7649
GA and SVM	95.24	0.9234

Compared with the KNN, RF and SVM methods, the proposed GA and SVM classification model showed the highest PA values (100%) on the testing dataset in different infection stages and the highest UA values (100%) on the testing dataset in the healthy, early and middle stages. Moreover, the proposed GA and SVM classification model provided the best accuracy (OA%: 95.24%, KAPPA: 0.9234). The results demonstrated that the collinearity existing between the spectral features usually deteriorated the performance of PWD infection stage identification, and the GA algorithm could select the optimal spectral features to present the dataset characteristics instead of using all 16 extracted spectral features. With the optimal spectral features (D_{green}, SD_{green}, D_{red}, D_{RE}, D_{NIR}, SD_{NIR}), the SVM parameters were also optimized and achieved better performance in the PWD infection stage detection than the KNN, RF and SVM classification models with 16 spectral features.

5. Discussion

Early detection is a topical issue in PWD control, and many studies focus on remote sensing. Ground remote-sensing methods collect data consisting of samples from the entire tree and provide more accurate data for individual pine trees. However, PWD usually affects trees in large areas, making ground-acquired data not feasible. Moreover, satellite remote sensing could collect large-scale data, but the low spatial resolution makes the individual tree discrimination impossible. Therefore, UAV remote sensing is a more promising and practical candidate for future large-scale forest management. For UAV remote sensing, data acquisition is easily affected by shadows, overlaps and weather conditions, which may induce measurement noise. In the future, more UAV data acquisition methods such as multispectral and LiDAR equipment will be combined to generate better PWD detection results.

The study results suggest that the accuracy of the GA and SVM classification model is higher than that of KNN, FR and SVM, which could extract spatial features from UAV HI. However, it failed to make full use of the spatial features of the HIs. On the other hand,

some studies employed 2D-CNNs, such as Faster R-CNN and YOLOv3, to extract spatial features such as color distribution and texture [12]; however, it failed to employ the spectral information. In recent years, the 3D-CNN has been extensively applied in HI classification in the forestry field [41]. It combines 1D spectral information and 2D spatial information, which could extract spectral and spatial features simultaneously, thus exhibiting great potential in monitoring PWD infections. Therefore, a 3D-CNN model on the HI will be examined in our future study to improve the accuracy of PWD detection.

6. Conclusions

It is known that the spectral characteristics of the pine trees change dramatically when the PWD infection of pine trees deteriorates. We extracted the pine tree crowns from the UVA-based HI and divided the PWD infection into four stages, namely, healthy, early, middle and serious stages, according to their physiological characteristics. A total of 16 spectral features were defined in the green region (510–580 nm), red edge (RE, 680–760 nm) and the near-infrared (NIR, 780–1000 nm) region, which were sensitive to the PWD infection. Then, we proposed a GA and SVM classification model for estimating the PWD infection stage of a pine tree with HI at tree level. In the evolution step of GA, the optimal spectral features were selected for training the SVM classification model with the highest fitness. We found that the proposed method increased the accuracy to 95.24% and the Kappa coefficient to 0.9234 compared with the KNN, RF and SVM classification models. We expect that the accuracy established here can be further improved by using a 3D-CNN model for estimating the PWD infection stage with both spectral and spatial information of the HI in the future.

Author Contributions: Conceptualization, S.Z.; methodology, H.H. and Y.H.; validation, D.C. and J.H.; writing—original draft preparation, S.Z.; writing—review and editing, H.H. All authors have read and agreed to the published version of the manuscript.

Funding: This work was supported in part by the National Natural Science Foundation of China under Grant 42071302, 62006029; in part by the Project of Chongqing Municipal Education Commission, China, under Grant KJQN202001442, KJQN202001434; in part by the Postdoctoral Innovative Talent Support Program of Chongqing under Grant CQBX2021024; in part by the Innovation Research Group of Chongqing Municipal Education Commission, China, under Grant CXQT20027; in part by the Education Reform and Research Project of Chongqing Municipal Education Commission, China, under Grant 202127; and in part by the College Students' Innovation and Entrepreneurship Project of Yangtze Normal University, Chongqing, China, under Grant 202210647006.

Institutional Review Board Statement: Not applicable.

Informed Consent Statement: Not applicable.

Data Availability Statement: Data available on request.

Conflicts of Interest: The authors declare no conflict of interest.

References

1. Kim, N.; Jeon, H.W.; Mannaa, M.; Jeong, S.-I.; Kim, J.; Kim, J.; Lee, C.; Park, A.R.; Kim, J.-C.; Seo, Y.-S. Induction of resistance against pine wilt disease caused by Bursaphelenchus xylophilus using selected pine endophytic bacteria. *Plant Pathol.* **2019**, *68*, 434–444. [CrossRef]
2. Rohdewald, P. A review of the French maritime pine bark extract (Pycnogenol), a herbal medication with a diverse clinical pharmacology. *Int. J. Clin. Pharmacol. Ther.* **2002**, *40*, 158–168. [CrossRef] [PubMed]
3. Park, Y.S.; Jeon, M.H.; Hwang, H.J.; Park, M.R.; Lee, S.H.; Kim, S.G.; Kim, M. Antioxidant activity and analysis of proanthocyanidins from pine (*Pinus densiflora*) needles. *Nutr. Res. Pract.* **2011**, *5*, 281–287. [CrossRef]
4. Yu, R.; Luo, Y.; Zhou, Q.; Zhang, X.; Wu, D.; Ren, L. A machine learning algorithm to detect pine wilt disease using UAV-based hyperspectral imagery and LiDAR data at the tree level. *Int. J. Appl. Earth Obs. Geoinf.* **2021**, *101*, 102363. [CrossRef]
5. Ikegami, M.; Jenkins, T.A.R. Estimate global risks of a forest disease under current and future climates using species distribution model and simple thermal model–Pine Wilt disease as a model case. *For. Ecol. Manag.* **2018**, *409*, 343–352. [CrossRef]
6. Ichihara, Y.; Fukuda, K.; Suzuki, K. Early symptom development and histological changes associated with migration of *Bursaphelenchus xylophilus* in seedling tissues of *Pinus thunbergii*. *Plant Dis.* **2000**, *84*, 675–680. [CrossRef]

7. Ye, J.R. Epidemic status of pine wilt disease in China and its prevention and control techniques and counter measures. *Sci. Silvae Sin.* **2019**, *55*, 1–10.
8. Sun, H.; Zhou, Y.; Li, X.; Zhang, Y.; Wang, Y. Occurrence of major forest pests in 2020 and prediction of occurrence trend in 2021 in China. *For. Pest Dis.* **2021**, *40*, 45–48.
9. Syifa, M.; Park, S.J.; Lee, C.W. Detection of the pine wilt disease tree candidates for drone remote sensing using artificial intelligence techniques. *Engineering* **2020**, *6*, 919–926. [CrossRef]
10. Zhao, B.G.; Futai, K.; Sutherland, J.R.; Takeuchi, Y. (Eds.) *Pine Wilt Disease*; Springer: Tokyo, Japan, 2008.
11. Zhang, S.; Huang, J.; Hanan, J.; Qin, L. A hyperspectral GA-PLSR model for prediction of pine wilt disease. *Multimed. Tools Appl.* **2020**, *79*, 16645–16661. [CrossRef]
12. Yu, R.; Luo, Y.; Zhou, Q.; Zhang, X.; Wu, D.; Ren, L. Early detection of pine wilt disease using deep learning algorithms and UAV-based multispectral imagery. *For. Ecol. Manag.* **2021**, *497*, 119493. [CrossRef]
13. Zhang, S.-L.; Qin, J.; Tang, X.-D.; Wang, Y.-J.; Huang, J.-L.; Song, Q.-L.; Min, J.-Y. Spectral characteristics and evaluation model of Pinus Massoniana suffering from Bursaphelenchus Xylophilus disease. *Spectrosc. Spectr. Anal.* **2019**, *39*, 865–872.
14. Kim, S.-R.; Lee, W.-K.; Lim, C.-H.; Kim, M.; Kafatos, M.C.; Lee, S.-H.; Lee, S.-S. Hyperspectral analysis of pine wilt disease to determine an optimal detection index. *Forests* **2018**, *9*, 115. [CrossRef]
15. Yu, R.; Ren, L.; Luo, Y. Early detection of pine wilt disease in Pinus tabuliformis in North China using a field portable spectrometer and UAV-based hyperspectral imagery. *For. Ecosyst.* **2021**, *8*, 44. [CrossRef]
16. Zhan, Z.; Yu, L.; Li, Z.; Ren, L.; Gao, B.; Wang, L.; Luo, Y. Combining GF-2 and Sentinel-2 images to detect tree mortality caused by red turpentine beetle during the early outbreak stage in North China. *Forests* **2020**, *11*, 172. [CrossRef]
17. Zhang, B.; Ye, H.; Lu, W.; Huang, W.; Wu, B.; Hao, Z.; Sun, H. A Spatiotemporal Change Detection Method for Monitoring Pine Wilt Disease in a Complex Landscape Using High-Resolution Remote Sensing Imagery. *Remote Sens.* **2021**, *13*, 2083. [CrossRef]
18. Li, X.; Tong, T.; Luo, T.; Wang, J.; Rao, Y.; Li, L.; Jin, D.; Wu, D.; Huang, H. Retrieving the Infected Area of Pine Wilt Disease-Disturbed Pine Forests from Medium-Resolution Satellite Images Using the Stochastic Radiative Transfer Theory. *Remote Sens.* **2022**, *14*, 1526. [CrossRef]
19. Santoso, H.; Tani, H.; Wang, X. A simple method for detection and counting of oil palm trees using high-resolution multispectral satellite imagery. *Int. J. Remote Sens.* **2016**, *37*, 5122–5134. [CrossRef]
20. Tang, L.; Shao, G. Drone remote sensing for forestry research and practices. *J. For. Res.* **2015**, *26*, 791–797. [CrossRef]
21. Ren, W.; Wu, D.; Qin, L. Preliminary Study on Data Collecting and Processing of Unmanned Airship Low Altitude Hyperspectral Remote Sensing. *Ecol. Environ. Monit. Three Gorges* **2016**, *1*, 52–57.
22. Wu, W.; Zhang, Z.; Zheng, L.; Han, C.; Wang, X.; Xu, J.; Wang, X. Research progress on the early monitoring of pine wilt disease using hyperspectral techniques. *Sensors* **2020**, *20*, 3729. [CrossRef] [PubMed]
23. You, J.; Zhang, R.; Lee, J. A Deep Learning-Based Generalized System for Detecting Pine Wilt Disease Using RGB-Based UAV Images. *Remote Sens.* **2021**, *14*, 150. [CrossRef]
24. Qin, L.; Wang, X.; Jiang, J.; Yang, X.; Ke, D.; Li, H.; Wang, D. Use hyperspectral remote sensing technique to monitoring pine wood nomatode disease preliminary. In *Hyperspectral Remote Sensing Applications and Environmental Monitoring and Safety Testing Technology*; SPIE: Bellingham, WA, USA, 2016; Volume 10156, pp. 410–414.
25. Huang, H.H.; Ma, X.H.; Huang, H.Y.; Zhou, Y.F.; Zhang, W.; Huang, Y.H. A preliminary study on monitoring of dead pine trees caused by pine wilt disease with fixed-wing unmanned aerial vehicle. *J. Environ. Entomol.* **2018**, *40*, 306–313.
26. Li, H.; Xu, H.H.; Zheng, H.Y.; Chen, X.Y. Monitoring technology of pine wilt disease based on UAV remote sensing image. *J. Chin. Agric. Mech.* **2020**, *41*, 170–175.
27. Abdel-Rahman, E.M.; Mutanga, O.; Adam, E.; Ismail, R. Detecting Sirex noctilio grey-attacked and lightning-struck pine trees using airborne hyperspectral data, random forest and support vector machines classifiers. *ISPRS J. Photogramm. Remote Sens.* **2014**, *88*, 48–59. [CrossRef]
28. Iordache, M.D.; Mantas, V.; Baltazar, E.; Pauly, K.; Lewyckyj, N. A machine learning approach to detecting pine wilt disease using airborne spectral imagery. *Remote Sens.* **2020**, *12*, 2280. [CrossRef]
29. Van Nguyen, T.; Park, Y.-S.; Jeoung, C.-S.; Choi, W.-I.; Kim, Y.-K.; Jung, I.-H.; Shigesada, N.; Kawasaki, K.; Takasu, F.; Chon, T.-S. Spatially explicit model applied to pine wilt disease dispersal based on host plant infestation. *Ecol. Model.* **2017**, *353*, 54–62. [CrossRef]
30. Yu, X.Z.; Wang, R.R.; Chen, W.J. Forest canopy segmentation by UAV remote sensing images using an improved watershed algorithm. *J. Fujian Agric. For. Univ. Nat. Sci. Ed.* **2018**, *47*, 428–434.
31. Xu, H.C.; Luo, Y.Q.; Zhang, T.T.; Shi, Y.J. Changes of reflectance spectra of pine needles in different stage after being infected by pine wood nematode. *Spectrosc. Spectr. Anal.* **2011**, *31*, 1352–1356.
32. Dos Santos, C.S.S.; de Vasconcelos, M.W. Identification of genes differentially expressed in Pinus pinaster and Pinus pinea after infection with the pine wood nematode. *Eur. J. Plant Pathol.* **2012**, *132*, 407–418. [CrossRef]
33. Mullen, K. Early Detection of Mountain Pine Beetle Damage in Ponderosa Pine Forests of the Black Hills Using Hyperspectral and WorldView-2 Data. Master's Thesis, Minnesota State University, Mankato, MN, USA, 2016; pp. 58–60.
34. Haboudane, D.; Miller, J.R.; Pattey, E.; Zarco-Tejada, P.J.; Strachan, I.B. Hyperspectral vegetation indices and novel algorithms for predicting green LAI of crop canopies: Modeling and validation in the context of precision agriculture. *Remote Sens. Environ.* **2004**, *90*, 337–352. [CrossRef]

35. Nijat, K.; Shi, Q.; Wang, J.; Rukeya, S.; Ilyas, N.; Gulnur, I. Estimation of spring wheat chlorophyll content based on hyperspectral features and PLSR model. *Trans. Chin. Soc. Agric. Eng.* **2017**, *33*, 208–216.
36. Wu, N.; Liu, J.; Yan, R. Using spectral feature parameters to estimate the chlorophyll content of Chinese fir under disease stress. *Plant Prot.* **2012**, *38*, 72–76.
37. Huang, M.; Gong, J.; Li, S.; Zhang, B.; Hao, Q. Study on pine wilt disease hyper-spectral time series and sensitive features. *Remote Sens. Technol. Appl.* **2013**, *27*, 954–960.
38. Guo, T.; Han, L.; He, L.; Yang, X. A GA-based feature selection and parameter optimization for linear support higher-order tensor machine. *Neurocomputing* **2014**, *144*, 408–416. [CrossRef]
39. Cortes, C.; Vapnik, V. Support-vector networks. *Mach. Learn.* **1995**, *20*, 273–297. [CrossRef]
40. Tu, B.; Wang, J.; Kang, X.; Zhang, G.; Ou, X.; Guo, L. KNN-based representation of superpixels for hyperspectral image classification. *IEEE J. Sel. Top. Appl. Earth Obs. Remote Sens.* **2018**, *11*, 4032–4047. [CrossRef]
41. Zhang, B.; Zhao, L.; Zhang, X. Three-dimensional convolutional neural network model for tree species classification using airborne hyperspectral images. *Remote Sens. Environ.* **2020**, *247*, 111938. [CrossRef]